Polymer 51 (2010) 2643–2651

Contents lists available at ScienceDirect

Polymer

journal homepage: www.elsevier.com/locate/polymer

Rheological behaviors and electrical conductivity of epoxy resin nanocomposites suspended with in-situ stabilized carbon nanofibers

Jiahua Zhu [a], Suying Wei [b], Atarsingh Yadav [a], Zhanhu Guo [a,*]

[a] Integrated Composites Laboratory (ICL), Dan F Smith Department of Chemical Engineering, Lamar University, Beaumont, TX 77710, USA
[b] Department of Chemistry and Physics, Lamar University, Beaumont, TX 77710, USA

ARTICLE INFO

Article history:
Received 9 March 2010
Received in revised form
1 April 2010
Accepted 10 April 2010
Available online 18 April 2010

Keywords:
Polymer nanocomposites
Rheology
Electrical conductivity

ABSTRACT

Epoxy resin nanocomposites suspended with carbon nanofibers (CNFs) have been prepared. A bifunctional coupling agent, 3-aminopropyltriethoxysilane, is used to treat the acid oxidized fibers. The dispersion quality of the CNFs with and without surface modification is monitored by an oscillatory rheological investigation. The addition of fibers is observed to influence the rheological behaviors of the suspensions drastically. Newtonian fluid behavior disappears as the fiber loading increases. A significant increase of the complex viscosity and storage modulus is observed, especially when the temperature increases to 50 °C and 75 °C. In-situ reaction between the amine-terminated functional groups on the silanized fibers and the resin, is justified by the FT-IR analysis and is responsible for the improved fiber dispersion and network formation. A decreased rheological percolation is observed after silanization due to the improved fiber dispersion quality. The electrical conductivity percolation is well correlated to the rheological percolation for the as-received fiber resin suspensions. However, with an insulating organic coating on the fiber surface, the conductivity increases slightly and lacks the correlation to the rheological percolation.

1. Introduction

Polymer nanocomposites (PNCs) have aroused great interest in materials science and engineering for their wide potential applications such as energy storage devices [1,2], electronics [3–6], sensors [7–11], and aerospace vehicles [12–15]. Among all the species of carbon-based nanomaterials, carbon nanotubes (CNTs) are obviously favored by most of the researchers owing to their unique mechanical and electrical properties [16–19]. However, carbon nanofibers (CNFs) with relatively lower manufacturing cost and fairly good electrical conductivity are promising fillers for fabricating structural PNCs [20]. The inert surface and large aspect ratio of CNFs and CNTs challenge the uniform dispersion. Various physicochemical methods have been used to introduce functional groups with an aim to improve their interfacial compatibility with polymer matrix [21–23]. For example, carboxylic acid group is formed as a result of the oxidation by strong nitric or sulfuric acid, and allows further surface functionality manipulation with either surfactants or coupling agents [21,24]. Unique properties are observed. For example, lower electrical percolation is observed for graphite-poly (methyl methacrylate) [25] and CNTs-epoxy composites [26].

Rheology is mostly oriented for better understanding of the fluid dynamics of the confined polymers [27,28]. Researchers recognize the rheological measurement as the most sensitive method for PNCs characterization over the most commonly used transmission electron microscopy and X-ray diffraction [29]. Dynamic rheology has been used to estimate the dispersion quality of CNTs in a polystyrene matrix [30]. Lozano et al. [31] observed a rheological threshold between 10 and 20 wt% for the melted CNFs/polypropylene PNCs. The rheological percolation has been correlated to the electrical percolation in the CNTs/polystyrene PNCs [16,32], mechanical properties of copper nanowire/polystyrene PNCs [33,34], and microwave properties in acrylic, polyurethane, and epoxy composites [35]. A gelation of 1.6 wt% CNTs in polycarbonate coincides with both the electrical percolation and the highest strength [36]. Until now, most of the reported researches focus on the study of thermoplastic PNCs [37–44]. And less work had been reported on the thermosetting PNCs [45,46]. Kotsilkova et al. introduce two critical concentrations [47,48]. The first (flocculation) depicts the critical concentration of local percolation and formation of fractal flocs. The second represents the formation of a continuous structural network of fractural flocs. Both are determined from the rheology data obtained from the low amplitude oscillatory shear flow test [49].

The present work reports on the investigation of the rheological and electrical conductive behaviors of resin nanocomposite suspensions with CNFs. The amine groups, introduced through the

* Corresponding author. Tel.: +1 409 880 7654; fax: +1 409 880 7283.
E-mail address: zhanhu.guo@lamar.edu (Z. Guo).

0032-3861/$ – see front matter © 2010 Elsevier Ltd. All rights reserved.
doi:10.1016/j.polymer.2010.04.019

silanization between carboxylic acid groups on the CNFs and 3-aminopropyltriethoxysilane (APTES), in-situ react with resin, which favors fiber dispersion and improves the interfacial interaction between fibers and resin. The surface functionality of the fibers is investigated by FT-IR spectroscopy. The effects of particle loading, surface treatment and operating temperatures on the complex viscosity, storage modulus and loss modulus are systematically studied. Both the rheological and electrical percolation values of the resin nanocomposite suspensions with the as-received and silanized fibers are comparatively studied.

2. Experimental

2.1. Materials

The epoxy resin used is Epon 862 (bisphenol F epoxy, Miller-Stephenson Chemical Company, Inc.). Vapor grown carbon nanofibers (CNFs, grade PR-24-XT-LHT, Pyrograf Products, Inc.) are heat treated at about 1500 °C to convert the deposited carbon present on the fiber surface to a short range ordered structure, aiming to provide higher electrical conductivity. The CNFs are reported to have an average diameter of 150 nm and length of 50–200 μm. The coupling agent, 3-aminopropyltriethoxysilane (APTES, 99%), is purchased from Sigma–Aldrich. Concentrated nitric acid and ethanol are provided from Thermo Fisher Scientific Inc. All the chemicals are used as-received without any further treatment.

2.2. Functionalization and characterization of carbon nanofibers

2.2.1. Oxidation

CNFs are oxidized in concentrated nitric acid under mechanical stirring at room temperature for half an hour. De-ionized water is used to wash the filtrate until it has a pH value of approximately 7. Then the obtained CNFs are dried in a vacuum oven at 80 °C over night and ready for silanization [50].

2.2.2. Silanization

The oxidized CNFs are dispersed in toluene rather than water under sonication for 1 h to prevent the loss of the APTES function [51]. APTES (1 wt%) is subsequently added into the above solution. The mixture is heated to 110 °C and refluxed for 8 h. The silanized CNFs are then filtrated and washed with DI water, ethanol and acetone in sequence for several times. The final product is dried in vacuum oven at 80 °C over night.

To investigate the surface functionalities of the CNFs after oxidation and silanization processes, Fourier transform infrared spectroscopy (FT-IR, Bruker Inc. Vector 22 FT-IR spectrometer, coupled with an ATR accessory) is used to characterize the as-received, oxidized and silanized CNFs in the range of 500–4000 cm^{-1} at a resolution of 4 cm^{-1}. The surface structure of the CNFs is investigated by scanning electron microscopy (Hitachi S-3400 scanning electron microscopy).

2.3. Preparation of CNFs-epoxy suspension and dispersion quality examination

Epoxy resin suspensions are prepared by incorporating 0.1, 0.3, 0.5, 1.0, 1.5, 2.0, and 2.5 wt% of the as-received and silanized CNFs into the liquid epoxy resin, respectively. The mixture is kept over night without stirring to wet the CNFs surface completely by monomers. High-speed (600 rpm) mechanical stirring is then performed at room temperature and followed by sonification for 1 h at room temperature.

The dispersion quality of the CNFs with and without surface treatment in the resin is monitored by microscopes (Olympus SZX 7 and Leitz wetzlar).

2.4. Rheological and electrical conductivity exploration of the nanocomposite suspensions

Dynamic rheological measurements are performed using an AR 2000ex Rheometer with an environmental test chamber (ETC, −160 °C to 600 °C, TA Instrumental Company). A series of measurements are performed in a cone-plate geometry with a diameter of 40 mm and a truncation of 64 μm. The measurements are done at 25 °C, 50 °C and 75 °C, respectively. Frequency sweeping between 0.1 and 100 rad/s is carried out at a low strain (1%), which is justified to be within the linear viscoelastic (LVE) range. The LVE range is determined by the strain-storage modulus (G') curve within the strain range from 0.01% to 100% at a frequency of 1 rad/s. Specimens placed between the cone and plate are allowed to equilibrate for about 2 min prior to each frequency sweeping.

The electrical conductivity of each suspension is measured by a four-probe technique in a Keithley 2400 SourceMeter under voltage-source testing mode. The measured voltage is adjusted in the range of −10 V to 10 V. The corresponding current is measured and recorded across the two outer probes.

Electrical resistivity (ρ, Ω cm) is calculated according to Equation (1) [52–54]

$$\rho = \frac{V \times 2\pi}{I \times \left(\frac{1}{S_1} + \frac{1}{S_2} - \frac{1}{S_1+S_2} - \frac{1}{S_2+S_3}\right) \times CF} \tag{1}$$

where, V is the potential difference between the two inner probes (V), I is the electrical current (A) that flows through the outer pairs of probes, S_n represents the distance (cm) between the two adjacent probes and CF is the correction factor that depends on sample thickness (W, cm) and S_n. In this case, ρ is measured after placing the solution in a non-conducting container with a fixed thickness. This corresponds to the seventh case reported by Valdes [52], for which the CF is shown in Equation (2).

$$CF = 1 + 4\frac{S}{W}\sum_{n=1}^{\infty}\left(\frac{1}{\sqrt{\left(\frac{S}{W}\right)^2+4n^2}} - \frac{1}{\sqrt{\left(\frac{2S}{W}\right)^2+4n^2}}\right) \tag{2}$$

where, S is the average distance among the probes, and W is the thickness of the solution. Thus, the electrical conductivity (σ, S/cm) is obtained by Equation (3):

$$\sigma = 1/\rho \tag{3}$$

3. Results and discussion

The surface functionalities of the CNFs before and after treatment are investigated by FT-IR. Fig. 1(A) shows the FT-IR spectra of the as-received, oxidized and silanized CNFs. The C–H stretching bands in the region of 3000–2800 cm^{-1} and the double CO_2 bands around 2350 cm^{-1} are observed in all the three samples. Due to the hydrogen bonding, carboxylic acid groups in the solid phase exhibit a broad band at ~3300 cm^{-1} corresponding to O–H stretching. The carboxylic acid group, C=O stretching band at 1678 cm^{-1} and the broad carboxylic acid OH deformation band at around 890 cm^{-1} verify the successful carboxylation/oxidation of the fibers. The band at 1585 cm^{-1} represents the primary amine of APTES [24].

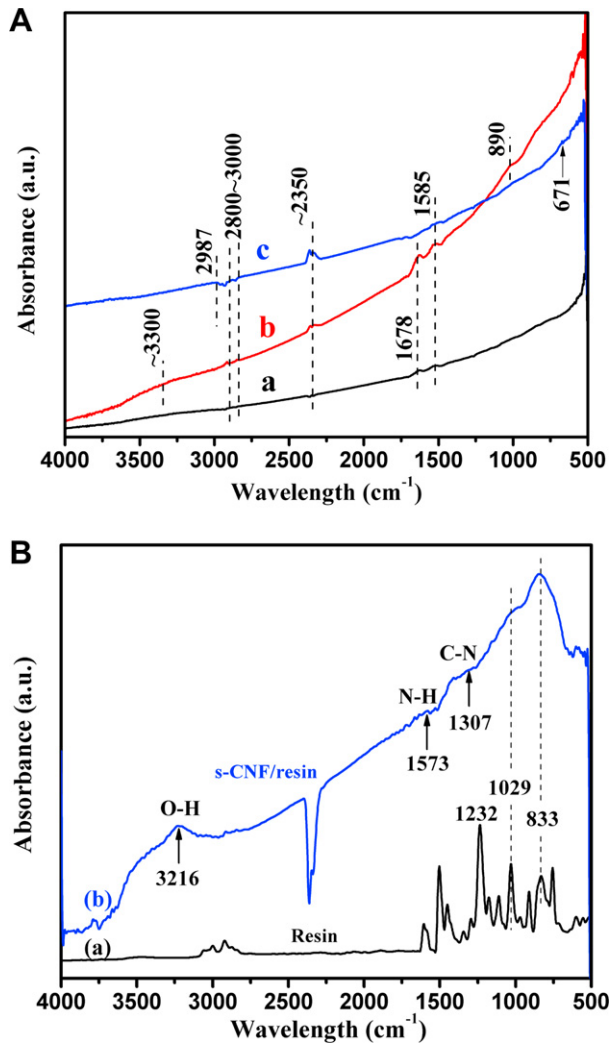

Fig. 1. FT-IR spectra of (A) (a) as-received, (b) oxidized and (c) silanized CNFs; and (B) (a) pure resin and (b) silanized fibers after 2-h reaction with resin at 120 °C.

Additional CH band at around 2987 cm^{-1} and weak N–H bending bonds [55] at 671 cm^{-1}, observed in the silanized rather than in the as-received and oxidized fibers, indicate that APTES has been covalently linked to the fibers. In summary, the carboxylic acid groups (–COOH) on the fiber surface after oxidation react with the ethoxyl groups of APTES to introduce amine groups on the fiber surface through the refluxing silanization process [39].

Fig. 2 (a–c) shows the microstructure of the as-received, oxidized and silanized fibers. The surfaces of the as-received CNFs are smooth, Fig. 2(a), and become relatively rough after acid treatment, Fig. 2(b) due to the strong acid etching. After acid oxidation and silanization, CNFs are observed to be wrapped with a thin layer and small pallet-like particles of the hydrolyzed APTES, Fig. 2(c). The fiber dimensions are observed unchanged under extensive SEM observations. The ultrasonic bath with a low power is able to disperse the CNFs without shortening the fiber length, which is consistent with the unchanged dimensions of the CNTs after the oxidation and silanization [56] and different from the shortening of the CNFs with the powerful ultrasonication horn [57,58].

The introduced carboxylic groups after acid oxidation are inert to the resin, and the only possible bonding is from weak hydrogen rather than strong chemical bonding between resin and oxidized CNFs, which is similar to ceramic nanoparticles filled vinyl ester resin PNCs [59–61]. Considering the nature of the hydroxyl groups of nanoparticles and the curing requirement of the carbon–carbon double bond in the vinyl ester resin, (3-methacryloxypropyl) trimethoxysilane (MPS) is used as a coupling agent to introduce the double bonds on the nanoparticle surface through the silanization reaction while the other side forms chemical bonding with the nanoparticles. The double bonds on the nanoparticle surface thus react with the vinyl ester upon catalysis to form the PNCs with an improved mechanical, optical and photoluminescent properties [59–61]. Similarly, APTES with bifunctional groups of hydrolysable group ($-Si(OCH_3)_3$) and amine group has been used as a coupling agent for functionalization of different nanomaterials such as TiO_2 [62,63], Fe_3O_4 [64], and CNTs [56] to introduce amine functional groups. The first functional group can be hydrolyzed and chemically bound to the oxidized fiber surface while the latter can serve as catalyst and be copolymerized with the resin to form a nanocomposite. Fig. 1(B) shows the FT-IR spectra of pure resin and the silanized fibers after reaction with resin at 120 °C for 5 h. The extra physical attached resin is removed by washing with acetone and dried in vacuum over night at 60 °C. The peaks at 3216 and 1573 cm^{-1} represent O–H and N–H groups, respectively. Meanwhile, the peaks at 1029 and 833 cm^{-1} are from the stretching of methyl groups and vibration of the benzene structure in both curves. These confirm the interfacial reaction between the amine group on the silanized fiber and epoxide group in resin during heating. Scheme 1 illustrates the oxidation, silanization of fibers, and in-situ reaction between the silanized fibers and the epoxy resin. Thus, only the silanized and as-received CNFs are used and compared for the subsequent tests.

3.1. Complex viscosity

3.1.1. Effect of fiber loading

Fig. 3 shows the complex viscosity (η^*) of the pure resin and CNFs-resin suspensions. In the suspensions with both the as-received and surface-treated CNFs, the increase of η^* with an increase of the CNFs loading especially at low frequencies is observed and is primarily due to the significant increase of the storage modulus G' and loss modulus G'' ($\eta^* = \eta' - i\eta''$, where $\eta' = G''/\omega$, $\eta'' = G'/\omega$. ω is angular frequency, rad/s) [65]. G' and G'' are discussed in Section 3.2.

Pure resin is observed to have frequency independent fluid properties, i.e., Newtonian-type flow. Shear thinning (viscosity decreases with an increase of shear rate/frequency) is observed in all the suspensions [66,67]. As the frequency becomes larger, the difference of η^* between the suspensions with the as-received and silanized fibers becomes diminished due to more similar dispersion quality from high-frequency shear stirring [48,68,69]. In the suspensions with a fiber loading of 0.5%, η^* decreases sharply with the increase of the frequency and reaches a value equal to that of pure resin. This indicates a Newtonian behavior of the suspension at higher frequency and a fluid rather than filler dominating fluid dynamics. The suspensions with a fiber loading higher than 0.5 wt% are orders of magnitude more viscous than that of the pure resin at lower frequency and exhibit stronger shear thinning behavior. These observations are in good agreement with the theoretical expectations for fiber reinforced composites [70] and the experimental observations in CNTs/polycarbonate PNCs [71]. However, no Newtonian plateau is observed in the resin suspensions with fiber loading higher than 0.5%. In the suspensions with loading above 1.5 wt%, the viscosity curves are almost linear over the whole frequency range. The initiating frequency to show the shear thinning increases with the increase of the CNFs loading (0.1 rad/s for pure monomers, 1.1 rad/s for solution suspended with 0.5 wt%, and even higher for solutions with higher loadings).

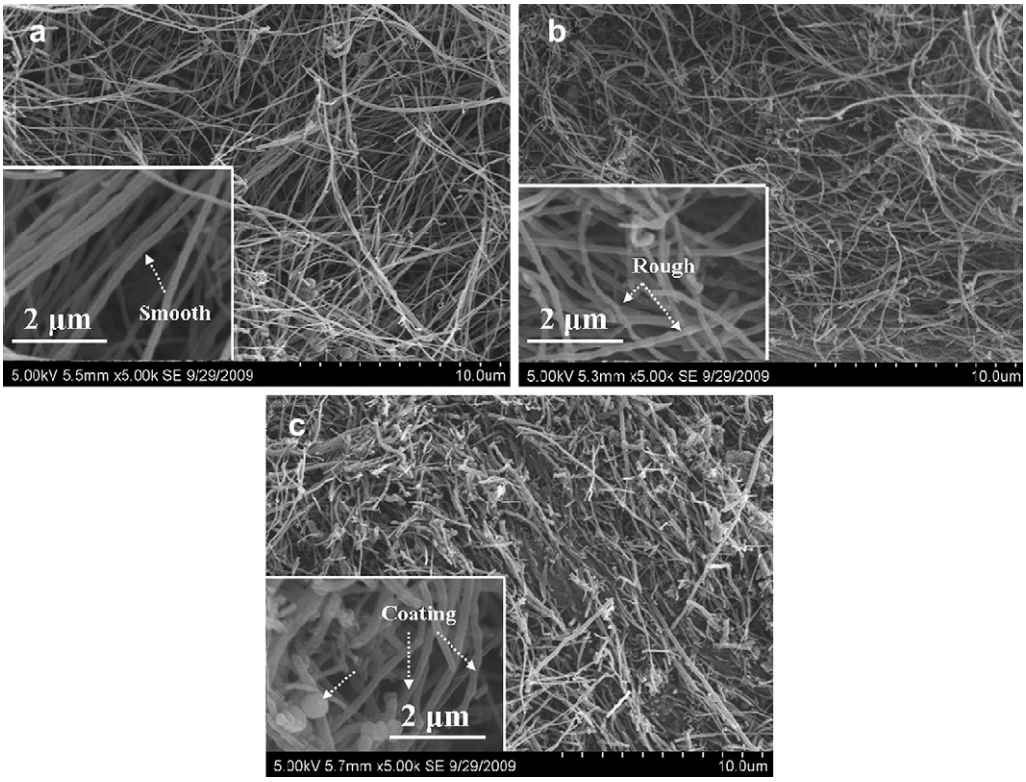

Fig. 2. SEM images of the (a) as-received, (b) oxidized and (c) silanized CNFs.

3.1.2. Effect of fiber surface modification

η^* of the resin suspensions with the as-received and modified fibers is comparatively studied at 25 °C with different frequencies, Fig. 3. The modified fibers exhibit a slightly decreased η^* under almost all the tested frequencies. After silanization, the anchored APTES on the fiber surface introduce an additional "soft layer", which prevents the agglomeration of fibers and subsequently improves the dispersion quality, Fig. 4. An increased viscosity with an improved dispersion quality by further exfoliation of organoclays is observed and is due to the increased 2-dimensional confinement of polymer chains [72,73]. Recently, a reduced viscosity with a better nanoparticle dispersion is reported in the fullerene and magnetite nanoparticles in polystyrene [68] and polystyrene nanoparticles in a linear polystyrene [74]. These reduced viscosity observations are due to the slip and or inhomogeneous flow [68,74] and higher viscosity is due to the nanoparticle agglomerates [68,74]. Meanwhile, a reduced viscosity is observed in the Fe_3O_4 nanoparticles suspended in polyacrylonitrile DMF

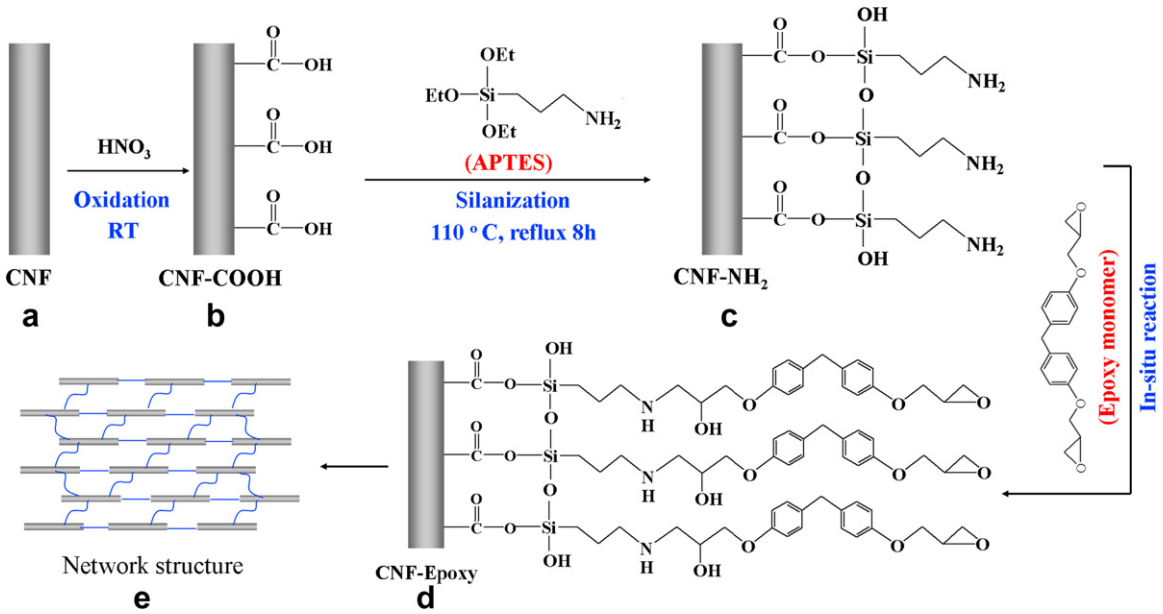

Scheme 1. Schemes of oxidation, silanization and in-situ reaction stabilization mechanisms.

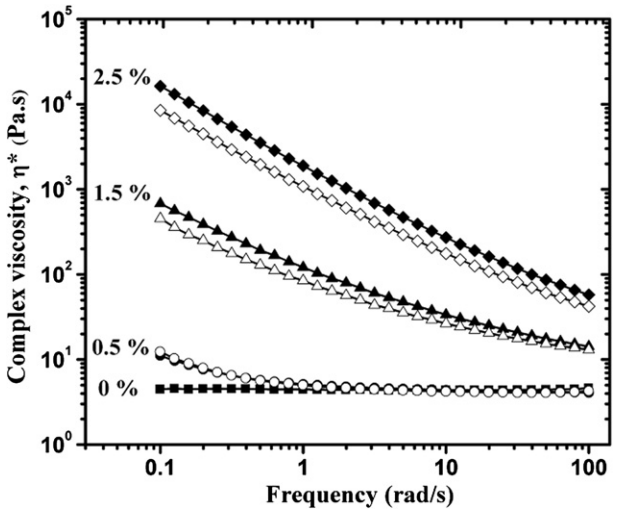

Fig. 3. Complex viscosity versus frequency of resin suspension with CNFs at 25 °C (Solid symbols: as-received CNFs; Open symbols: silane modified CNFs).

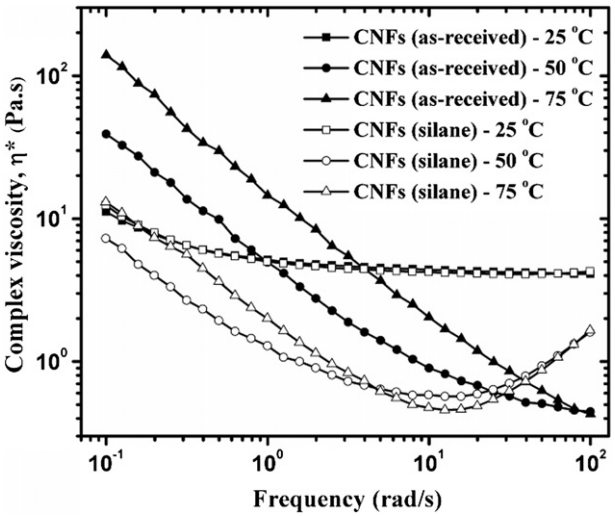

Fig. 5. Complex viscosity (η^*) as a function of frequency at different temperatures (0.5 wt% CNFs).

solution, which is interpreted in terms of the enhanced orientated polymer chains [75,76]. In this work, the better fiber dispersion promotes the alignment of fibers, which makes resin easier to flow [75,76] and thus reduces the internal friction between polymer chains. Similar phenomenon is observed in the $CaCO_3$ particles dispersed in the polyethylene matrix [77] and poly(dimethyl siloxane) matrix [69], in which agglomerated clusters increase the viscosity and surface treatment reduces the viscosity with an improved particle dispersion [69,77].

3.1.3. Effect of temperature

Fig. 5 shows the temperature effect on η^* for the resin suspensions with both the as-received and silanized fibers. There is little rheological difference between the suspensions with the as-received and silanized fibers at 25 °C. η^* is observed to decrease sharply with an increase of the frequency in the lower frequency range (0.1–1 rad/s) and to decrease slowly in the higher frequency range (1–100 rad/s). However, η^* in the resin suspensions with silanized fibers at 50 °C and 75 °C is much lower in the lower frequency range and higher in the high-frequency range than those with the as-received fibers. η^* is observed to decrease with an initial increase of the frequency within the frequency of 0.1–15 rad/s and to increase significantly when the frequency exceeds 15 rad/s. The amine group on the silanized fibers in-situ reacts with the resin and a more rigid network structure is formed arising from the resin curing between the amine group on the silanized fibers and the resin at higher temperatures. The formed network restricts the relative motions of the fibers and resin and is responsible for the increased η^* at relatively high temperature.

The effect of the surface treatment on η^* is observed more significant at 50 °C and 75 °C. In the resin suspensions with the as-received fibers, η^* decreases during the frequency sweeping range. A higher η^* at 75 °C is observed than that at 50 °C in the resin suspensions with the as-received fibers in all the sweeping frequency range. However, in the resin suspension with surface-treated fibers, η^* at 75 °C is higher than that at 50 °C with frequency lower than 4 rad/s and then becomes minimum and almost equals to that at 50 °C with frequency larger than 10 rad/s. An almost equal η^* values at 50 °C and 75 °C are observed for resin suspensions with both the as-received and silanized CNFs in higher frequency range.

3.2. Storage modulus (G') and loss modulus (G'')

3.2.1. Effect of fiber loading

Fig. 6(a) and (b) shows the storage modulus (G', elastic property) and loss modulus (G'', viscous property) as a function of frequency. Both G' and G'' increase with an increase of the frequency. However, the rate of increase becomes slower in the resin suspensions with higher fiber loadings. The fiber loading is observed to have more impact on the modulus at low frequencies than that at high

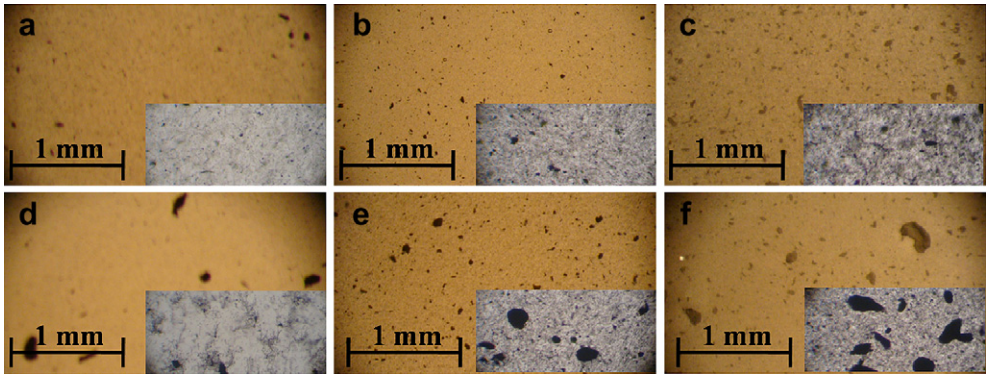

Fig. 4. Optical micrographs of epoxy suspension films filled with silane treated CNFs (a) 0.1 wt%, (b) 0.3 wt%, and (c) 0.5 wt%; and as-received CNFs (d) 0.1 wt%, (e) 0.3 wt%, and (f) 0.5 wt% (The images are taken by Olympus SZX 7 microscope, insets are the images with larger magnification taken by leitz wetzlar microscope).

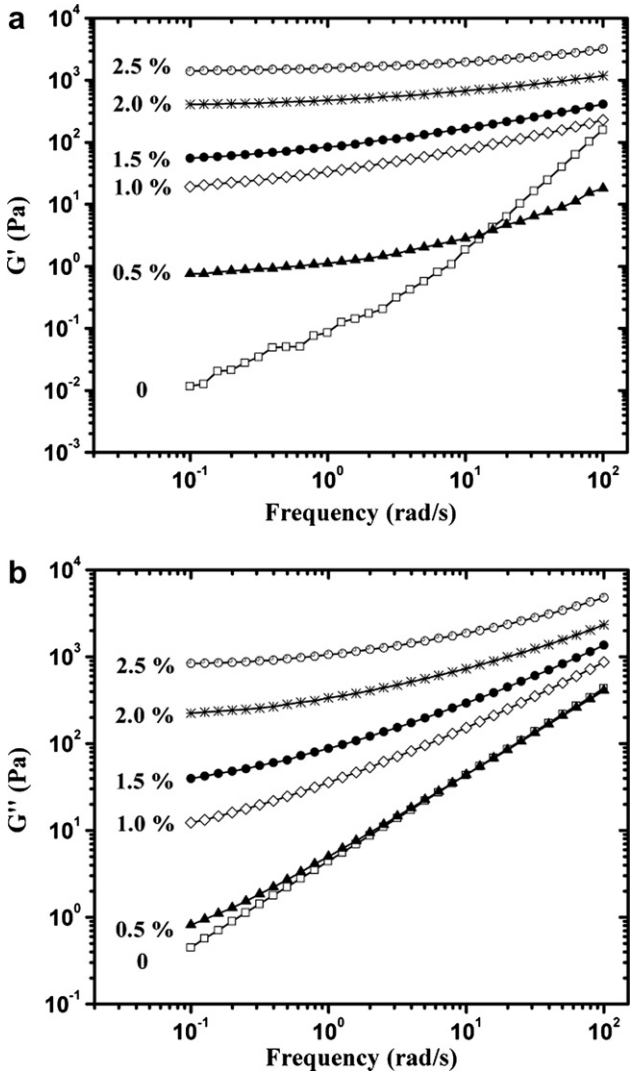

Fig. 6. (a) Storage modulus (G') and (b) loss modulus (G'') of resin nanocomposite suspensions with the as-received CNFs at 25 °C.

frequencies. For pure resin, G' curve has a much steeper slope in the whole sweeping frequency range. In the resin suspensions, G' and G'' increase significantly with the increase of fiber loading. Though the polymer chain interaction still exists, the introduced fiber–fiber and fiber–monomer interactions dominate and are responsible for the enhanced G' in the resin suspensions, especially with loading larger than 0.5 wt%. G' is observed to be almost independent of the frequency, when the fiber loading is above 2 wt%, which is due to the formed network structure [48].

It is well known that an inter-connected structure of anisometric fillers results in an apparent yield stress, which is a variable in dynamic measurements by a plateau of G' and G'' versus frequency at low frequencies [71,78]. The structural network is constructed by the intimate contact of the fillers, which are wrapped with the absorbed polymer [79]. Compared to the viscous G'', the elastic G' is found to be more sensitive to the dispersion quality of nanofillers, which is strongly dependent on the interfacial energy [78]. With the increase of the fiber loading, an inter-connected network structure in the solution is formed and this critical particle loading is regarded as a rheological percolation concentration [71]. In this work, even in the resin suspensions with a fiber loading of 0.5 wt%, G' is observed to exhibit a plateau, which indicates the formation of an inter-connected network structure. As the fiber loading further increases, the elastic behavior of the suspension is strengthened owning to the enhanced connectivity of the network.

3.2.2. Effect of surface modification

Fig. 7 shows the modulus versus frequency of the resin suspensions with the as-received and silanized fibers, respectively. The crossing point of the G' and G'' curves is used as a criteria to indicate a switch from viscous liquid to elastic solid behavior [80]. The crossing points of resin suspension with 0.5, 1.5 and 2.5 wt% of the as-received fibers are observed at 0.1, 0.8 and 12.0 rad/s, Fig. 7 (a), respectively. The suspension is observed to switch from viscous to elastic when the oscillatory frequency exceeds these crossing points. The crossing points decrease to 0.07, 0.3 and 8.0 rad/s for the suspensions with silanized fibers with a loading of 0.5, 1.5 and 2.5%, respectively. This change indicates that the suspensions with silanized fibers experience an earlier transition from viscous to elastic state. The plateau at low frequencies for G' curve indicates an inter-connected structure of nanofillers [71]. According to the curves in both Fig. 7(a) and (b), obvious plateaus are observed even at a low content of 0.5 wt% for the resin suspensions with both the

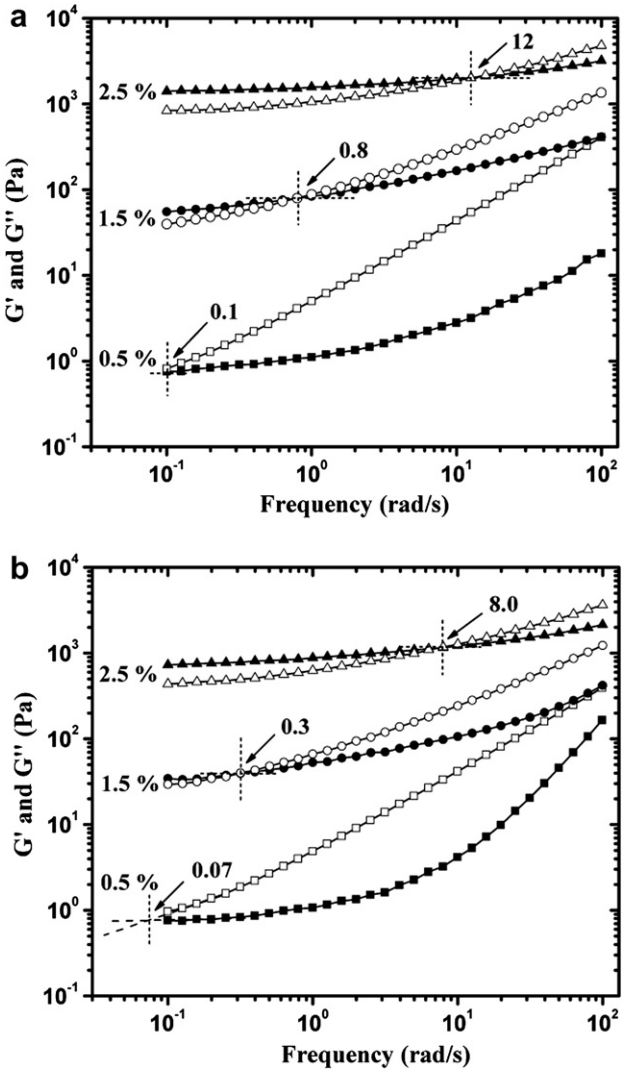

Fig. 7. Storage modulus G' (solid symbols) and loss modulus G'' (open symbols) versus frequency of resin suspensions with (a) as-received and (b) silanized CNFs at 25 °C.

as-received and modified fibers. Therefore, the rheological behaviors are dominated by the conformation structures of fibers in the suspensions. After silanization, the interfiber interaction decreases [77] and the network structure [48] is more sensitive to the external forces. And thus the earlier transition is observed and this result is consistent with the observed reduced η^* as discussed previously.

3.2.3. Effect of temperature

Fig. 8 shows the complex viscosity (η^*) versus frequency of the epoxy resin suspensions with a fiber loading of 1 wt% at different temperatures. Temperature is observed to have a significant effect on the modulus, especially the storage modulus (G'). In the epoxy resin suspensions with 1.0 wt% of the as-received fibers, G' is lower at 75 °C than that at 50 °C. As temperature increases, G' decreases owning to the polymer chain relaxation at high temperatures [77]. However, G' for the resin suspensions with the silanized fibers is much higher at 75 °C than that at 50 °C. With the increase of the temperature, the in-situ reaction between the silanized fibers and resin becomes much faster, forming stronger fiber–monomer and fiber–fiber entangling connections, Scheme 1. This formed network structure directly increases the elastic behavior of the suspension with an increased G' [81]. For the silanized fibers, the slope of G' curve is similar to that of the as-received fibers within the frequency range from 0.1 to 10 rad/s. As the frequency further increases, G' increases sharply in the resin suspensions with the silanized fibers at frequency higher than 10 rad/s. At 50 °C, G' is initially lower in the resin suspensions with the silanized fibers than that in the resin suspensions with the as-received fibers. This is due to a better dispersion arising from the nanofiber surface treatment [69]. However, as the in-situ reaction proceeds, G' exceeds that in the resin suspension with the as-received fibers when the frequency is above 13 rad/s. The motion of fibers is restricted in the local polymer domains by the formed rigid network structure after the in-situ reaction at higher temperatures [48,77].

3.3. Rheological percolation characterization

Kotsilkova et al. have introduced two critical concentrations, called the first and second percolation thresholds [47,48]. The first percolation threshold (flocculation, C*) depicts the critical concentration of local percolation and formation of fractal flocs. The second rheological threshold (percolation, C**) represents the formation of

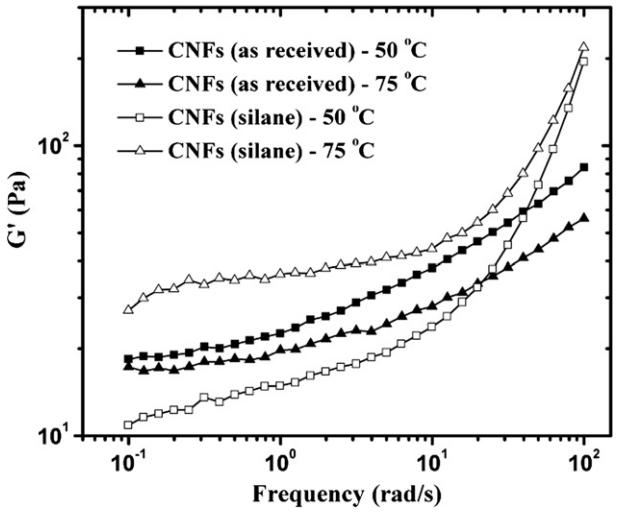

Fig. 8. Storage modulus G' of 1 wt% CNFs filled epoxy at 50 and 75 °C.

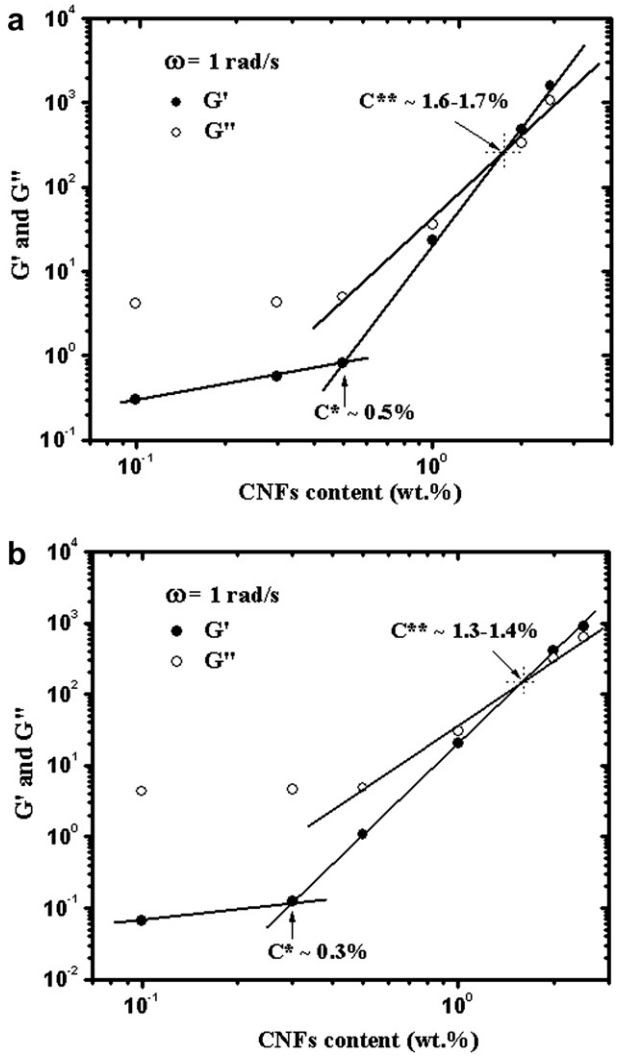

Fig. 9. Plot of G' and G'' at a low frequency ($\omega = 1$ rad/s) versus fiber loading in the resin suspension with (a) as-received and (b) silanized CNFs at 25 °C.

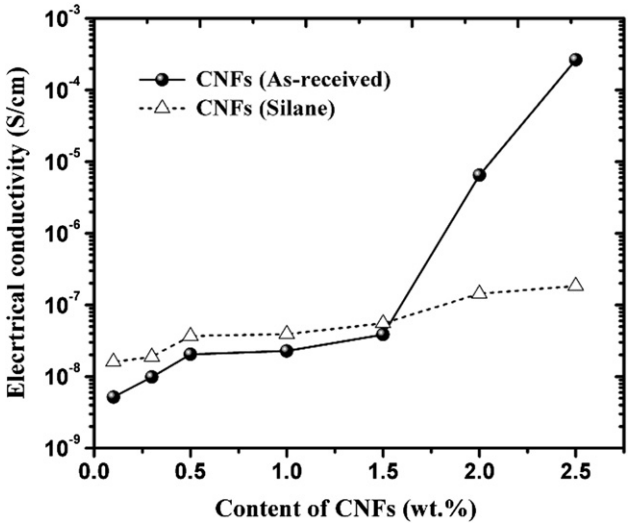

Fig. 10. Effect of CNFs loading on the electrical conductivity of epoxy resin nanocomposites.

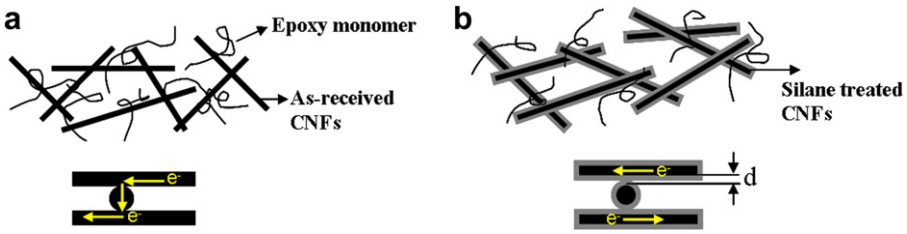

Fig. 11. Contact model of CNFs in epoxy solutions suspended with (a) as-received CNFs and (b) silane treated CNFs.

a continuous structural network of fractural flocs. Rheology method proposes an approach to determine the two thresholds using rheological data from the low amplitude oscillatory shear flow [49]. Most of the publications on the rheology of PNCs report on the percolation superstructure of the nanofillers and the construction of a relationship between the sharp change of the rheological properties and the percolation transitions [71,80]. In order to investigate the fiber surface modification effect on the percolation properties, the curves of low frequency G' and G'' at $\omega = 1$ rad/s for both the as-received and modified fibers are plotted and compared. C^* is determined by the crossing point of the two distinctive slopes of G'. And the crossing point of G' and G'' determines C^{**}. From Fig. 9(a), C^* and C^{**} of the suspensions with the as-received fibers are 0.5 wt% and 1.6–1.7 wt%, respectively. However, the two thresholds reduce to 0.3 wt% and 1.3–1.4 wt% after fiber silanization, Fig. 9(b). This is attributed to the enhanced dispersion quality of the modified fibers in the resin, which enhances the formation of the fiber interconnect and continuous network structure.

3.4. Electrical conductivity

Rheological transitions (percolation) are reported to be strongly related to other physical properties [32–35]. However, most of the physical properties are measured in the solid states, while rheological properties are conducted in the melt state of the thermoplastics [16,32,34]. In this work, both rheological property and electrical conductivity (σ) are tested in the resin suspensions. σ is observed lower for the resin suspension with the as-received fibers than that for the resin suspension with silanized fiber loading lower than 1.5 wt%. σ is observed to increase rapidly for the resin suspension with the as-received fibers with loadings higher than 1.5%, which is coincided with the second percolation threshold, Fig. 10. The sharply increase of σ is due to the formation of the interconnected network among fibers. Once the network formed, a pathway is created to facilitate the electron transportation among fibers. Similar results have been reported on CNTs/polycarbonate composites [36]. However, σ changes slightly with the increase of the fiber loading for the resin suspensions with the silanized fibers. Ma et al. [82] also found a decreased σ for the CNT/epoxy PNCs after CNT functionalization with organic agent. After surface modification, the fibers are coated with an organic layer, which prevents the direct contact between nanofibers. Therefore, the electron transport is blocked by the organic layer, schematically shown in Fig. 11. Thus, σ increases slightly (2.5%) even though the silanized fiber loading is much higher than the percolation concentration (1.3–1.4 wt%).

4. Conclusion

The complex viscosity increases significantly with the increase of the fiber loading. The viscosity increase is accompanied by an increase of the storage modulus. Surface modification with APTES improves the dispersion quality of CNFs in the resin. At high temperatures, the amine groups on the silanized CNFs in-situ react with resin and form a rigid network structure. The observed sharply increased complex viscosity and storage modulus indicate a dominating elastic rheological behavior at relative high oscillatory frequency. Lower rheological percolations, 0.3 wt% and 1.3–1.4 wt%, of the modified CNFs-epoxy resin suspensions are obtained as compared to 0.5 wt% and 1.6–1.7 wt% for the as-received CNFs-epoxy resin nanocomposites. The reported rheological investigation provides important information to control the film thickness for the epoxy nanocomposites fabrication by using especially the spin coating method [83–86]. The sharp increase of the electrical conductivity in the epoxy resin suspension with 1.5 wt% of the as-received CNFs well corresponds to the second rheological percolation value of 1.6–1.7 wt%. However, no electrical transition is observed for the resin suspensions with silanized fibers. Surface treatment improves the dispersion quality and stability of fibers in epoxy resin. However, the lower electrical conductivity in the silanized suspensions is due to the coated insulating organic layer.

Acknowledgement

This work is supported by the research start-up fund and research enhancement grant from Lamar University. The financial supports from Dan F. Smith Department of Chemical Engineering and College of Engineering at Lamar University for obtaining the TA rheometer are kindly acknowledged.

References

[1] Pushparaj VL, Shaijumon MM, Kumar A, Murugesan S, Ci L, Vajtai R, et al. PNAS 2007;104:13574–7.
[2] Kim P, Doss NM, Tillotson JP, Hotchkiss PJ, Pan M-J, Marder SR, et al. ACS Nano 2009;3:2581–92.
[3] Vacca P, Nenna G, Miscioscia R, Palumbo D, Minarini C, Sala DD. J Phys Chem C 2009;113:5777–83.
[4] Nogueira AF, Lomba BS, Soto-Oviedo MA, Correia CRD, Corio P, Furtado CA, et al. J Phys Chem C 2007;111:18431–8.
[5] Guo Z, Park S, Hahn HT, Wei S, Moldovan M, Karki AB, et al. J Appl Phys 2007;101:09M511.
[6] Guo Z, Lee SE, Kim H, Park S, Hahn HT, Karki AB, et al. Acta Mater 2009;57:267.
[7] Shimada T, Ookubo K, Komuro N, Shimizu T, Uehara N. Langmuir 2007;23:11225–32.
[8] Wen Z, Ci S, Li J. J Phys Chem C 2009;113:13482–7.
[9] Guo Z, Park S, Hahn HT, Wei S, Moldovan M, Karki AB, et al. Appl Phys Lett 2007;90:053111.
[10] Guo Z, Hahn HT, Lin H, Karki AB, Young DP. J Appl Phys 2008;104:014314.
[11] Zhang D, Chung R, Karki AB, Li F, Young DP, Guo Z. J Phys Chem C 2010;114:212–9.
[12] Hussain F, Hojjati M, Okamoto M, Gorga RE. J Compos Mater 2006;40:1511–75.
[13] Podsiadlo P, Kaushik AK, Arruda EM, Waas AM, Shim BS, Xu J, et al. Science 2007;318:80–3.
[14] Bonderer LJ, Studart AR, Gauckler LJ. Science 2008;319:1069–73.
[15] Munch E, Launey ME, Alsem DH, Saiz E, Tomsia AP, Ritchie RO. Science 2008;322:1516.
[16] Kota AK, Cipriano BH, Duesterberg MK, Gershon AL, Powell D, Raghavan SR, et al. Macromolecules 2007;40:7400–6.
[17] Sun L, Warren GL, O'Reilly JY, Everett WN, Lee SM, Davis D, et al. Carbon 2008;46:320–8.

[18] Warren GL, Sun L, Hadjiev VG, Davis D, Lagoudas D, Sue HJ. J Appl Polym Sci 2009;112:290–8.
[19] Sun L, Sue HJ. Epoxy/carbon nanotube nanocomposites. In: Pascault J-P, Williams RJJ, editors. Epoxy polymers: new materials and innovations. Weinheim, Germany: Wiley-VCH; 2010.
[20] Sun L, O'Reilly JY, Tien CW, Sue HJ. J Chem Educ 2008;85:1105–7.
[21] Tasis D, Tagmatarchis N, Bianco A, Prato M. Chem Rev 2006;106:1105–36.
[22] Yang Y, Xie X, Yang Z, Wang X, Cui W, Yang J, et al. Macromolecules 2007;40:5858–67.
[23] Mitchell CA, Krishnamoorti R. Macromolecules 2007;40:1538–45.
[24] Wang J, Fang Z, Gu A, Xu L, Liu F. J Appl Polym Sci 2006;100:97–104.
[25] Zheng W, Wong S-C. Compos Sci Technol 2003;63:225–35.
[26] Barrau S, Demont P, Perez E, Peigney A, Laurent C, Lacabanne C. Macromolecules 2003;36:9678–80.
[27] Krishnamoorti R, Vaia RA, Giannelis EP. Chem Mater 1996;8:1728–34.
[28] Krishnamoorti R, Giannelis EP. Macromolecules 1997;30:4097–102.
[29] Utracki LA. Clay-containing polymeric nanocomposites. Shawbury, shrewsbury, UK: Rapra Technology; 2004.
[30] Zhang Q, Fang F, Zhao X, Li Y, Zhu M, Chen D. J Phys Chem B 2008;112:12606–11.
[31] Lozano K, Bonilla-Rios J, Barrera EV. J Appl Polym Sci 2001;80:1162–72.
[32] Du F, Scogna RC, Zhou W, Brand S, Fischer JE, Winey KI. Macromolecules 2004;37:9048.
[33] Scott TK, Jack FD, Francis WS. J Polym Sci Part B: Polym Phys 2007;45:1882–97.
[34] Lin B, Gelves GA, Haber JA, Sundararaj U. Ind Eng Chem Res 2007;46:2481–7.
[35] Kotsilkova R, Nesheva D, Nedkov I, Krusteva E, Stavrev S. J Appl Polym Sci 2004;92:2220–7.
[36] Liu C, Zhang J, He J, Hu G. Polymer 2003;44:7529–32.
[37] Kim H, Macosko CW. Macromolecules 2008;41:3317–27.
[38] Panek G, Schleidt S, Mao Q, Wolkenhauer M, Spiess HW, Jeschke G. Macromolecules 2006;39:2191–200.
[39] Xu L, Nakajima H, Manias E, Krishnamoorti R. Macromolecules 2009;42:3795–803.
[40] Lee KM, Han CD. Macromolecules 2003;36:7165–78.
[41] Huang W, Han CD. Macromolecules 2006;39:257–67.
[42] Choi S, Lee KM, Han CD. Macromolecules 2004;37:7649–62.
[43] Zou H, Wu S, Shen J. Chem Rev 2008;108:3893–957.
[44] Xiao M, Sun L, Liu J, Li Y, Gong K. Polymer 2002;43:2245–8.
[45] Sun L, Boo WJ, Liu J, Clearfield A, Sue HJ, Verghese NE, et al. Macromol Mater Eng 2009;294:103–13.
[46] Wang H, Hoa SV, Wood-Adams PM. J Appl Polym Sci 2006;100:4286–96.
[47] Kotsilkova R. J Appl Polym Sci 2005;97:2499–510.
[48] Kotsilkova R, Fragiadakis D, Pissis P. J Polym Sci Part B: Polym Phys 2005;43:522–33.
[49] Kotsilkova R. sofia, Bulgaria; 2005. [D.Sc thesis, in Bulgarian].
[50] Seyhan AT, Sun Z, Deitzel J, Tanoglu M, Heider D. Mater Chem Phys 2009;118:234–42.
[51] Martin HJ, Schulz KH, Bumgardner JD, Walters KB. Langmuir 2007;23:6645–51.
[52] Valdes LB. Proc IRE 1954;42:420–7.
[53] De Souza Jr FG, Soares BG, Pinto JC. Eur Polym J 2008;44:3908–14.
[54] Zhu J, Wei S, Alexander Jr M, Cocke D, Ho TC, Guo Z. J Mater Chem 2010;20:568–74.
[55] Chong ASM, Zhao XS. J Phys Chem B 2003;107:12650–7.
[56] Kathi J, Rhee K. J Mater Sci 2008;43:33–7.
[57] Zhamu A, Hou YP, Zhong WH, Stone JJ, Li J, Lukehart CM. Polym Compos 2007;28:605.
[58] Li B, Sui G, Zhong WH. Adv Mater 2009;21:4176–80.
[59] Guo Z, Tony P, Oyoung C, Wang Y, Hahn HT. J Mater Chem 2006;16:2800–8.
[60] Guo Z, Lei K, Li Y, Ng HW, Hahn HT. Compos Sci Technol 2008;68:1513–20.
[61] Guo Z, Wei S, Shedd B, Scaffaro R, Pereira T, Hahn HT. J Mater Chem 2007;17:806–13.
[62] Song YY, Hildebrand H, Schmuki P. Surf Sci 2010;604:346–53.
[63] Martin HJ, Schulz KH, Bumgardner JD, Walters KB. Appl Surf Sci 2008;254:4599–605.
[64] Wu W, He Q, Chen H, Tang J, Nie L. Nanotechnology 2007;18:145609.
[65] Shenoy AV. Rheology of filled polymer systems. Kluwer Academic Publishers; 1999.
[66] Poslinski AJ, Ryan ME, Gupta RK, Seshadri SG, Frechette FJ. J Rheol 1988;32:703–35.
[67] Ugaz VM, Cinader DK, Burghardt WR. Macromolecules 1997;30:1527–30.
[68] Tuteja A, Duxbury PM, Mackay ME. Macromolecules 2007;40:9427–34.
[69] Kaully T, Siegmann A, Shacham D. Polym Adv Technol 2007;18:696–704.
[70] Mutel AT, Kamal MR. In: Utracki LA, editor. Two phase polymer systems, vol. 12. Munich: carl Hanser; 1991. p. 305–31.
[71] Pötschke P, Fornes TD, Paul DR. Polymer 2002;43:3247–55.
[72] Wagener R, Reisinger TJG. Polymer 2003;44:7513–8.
[73] Hyun YH, Lim ST, Choi HJ, Jhon MS. Macromolecules 2001;34:8084–93.
[74] Mackay ME, Dao TT, Tuteja A, Ho DL, Kim HC, Hawker CJ. Nat Mater 2003;2:762–6.
[75] Zhang D, Karki AB, Rutman D, Young DP, Wang A, Cocke D, et al. Polymer 2009;50:4189–98.
[76] Liu W, Cheng L, Zhang H, Zhang Y, Wang H, Yu M. Int J Mol Sci 2007;8:180–8.
[77] Osman MA, Atallah A. Polymer 2005;46:9476–88.
[78] Utracki LA. Polym Compos 1986;7:274–82.
[79] Kotsilkova R. Thermoset nanocomposites for engineering applications. Shawbury, shrewsbury, UK: Rapra Technology; 2007.
[80] Wooster TJ, Abrol S, MacFarlane DR. Polymer 2005;46:8011–7.
[81] Shih WH, Shih WY, Kim SI, Liu J, Aksay IA. Phys Rev A 1990;42:4772–9.
[82] Ma PC, Tang BZ, Kim JK. Carbon 2008;46:1497–505.
[83] Emslie AG, Bonner FT, Peck LG. J Appl Phys 1958;29:858–62.
[84] Meyerhofer D. J Appl Phys 1978;49:3993–7.
[85] Schwartz LW, Roy RV. Phys Fluids 2004;16:569–84.
[86] Zhu J, Wei S, Ryu J, Budhathoki M, Liang G, Guo Z. J Mater Chem, in press. doi: 10.1039/C0JM00063A